Investigation of Short Time Scale Variation of Solar Radiation Spectrum in UV, PAR, and NIR Bands due to Atmospheric Aerosol and Water Vapor

Jackson H. W. Chang, Jedol Dayou, and Justin Sentian

Abstract—Long terms variation of solar insolation had been widely studied. However, its parallel observations in short time scale is rather lacking. This paper aims to investigate the short time scale evolution of solar radiation spectrum (UV, PAR, and NIR bands) due to atmospheric aerosols and water vapors. A total of 25 days of global and diffused solar spectrum ranges from air mass 2 to 6 were collected using ground-based spectrometer with shadowband technique. The result shows that variation of solar radiation is the least in UV fraction, followed by PAR and the most in NIR. Broader variations in PAR and NIR are associated with the short time scale fluctuations of aerosol and water vapors. The corresponding daily evolution of UV, PAR, and NIR fractions implies that aerosol and water vapors variation could also be responsible for the deviation pattern in the Langley-plot analysis.

Keywords—Aerosol, short time scale variation, solar radiation, water vapor.

I. INTRODUCTION

SOLAR surface insolation represents the amount of solar radiance reaches the Earth's surface in a specified area. Ithas important implications in various fields such as solar renewable energy [1], meteorology [2], and climate change [3]. Previous studies revealed that there are several parameters affect the amount of solar radiation reaching the land surface.

Generally, cloudis the major modulator of solar radiation reaching the land surface. This is inferred from satellite data that showing increment in surface solar radiation at the rate of $0.16 W/m^2$ per year since 1990, which is consistent with the decreasing in cloudiness observed using similar instrument [4]. Under overcast condition, clouds have larger spatial and temporal than other atmospheric constituents, which reflect most of the incident solar radiation, reducing atmospheric transmittance and capture longwave radiation from land surface.

J. H. W. Chang is a postgraduate student with the e-VIBS research group, School of Science and Technology, UMS, Jalan UMS, 88400 Kota Kinabalu, Malaysia.(e-mail: jacksonchang87@gmail.com).
J. Dayouis an Associate Professor with the e-VIBS research group, School of Science and Technology, UMS, Jalan UMS, 88400 Kota Kinabalu, Malaysia. (phone: +6-088-320000 fax: +6-088-435324 e-mail: jed@ums.edu.my).
J. Sentian is a Senior Lecturer with the CCRG research group, School of Science and Technology, UMS, Jalan UMS, 88400 Kota Kinabalu, Malaysia. (e-mail: jsentian@ums.edu.my).

Under cloud-free condition, increased anthropogenic aerosol loading from emissions of pollutants could be responsible for decreased surface solar radiation [5]. This is because increased air pollutant may have produced a fog-like haze that reflected/absorbed radiation from sun and resulted in less solar radiation reaching the surface. Reference [3] however found that the negative surface solar radiation trends before 1990 in China which could be attributed to increase in aerosol loading, but failed to explain the trend reverses after 1986 while there was no sufficient evidence that aerosols are decreasing in those regions in the recent years.This is further verified in the Tibetan Plateau where the aerosol load contributed by human activities were still negligible, but its decreasing rate in solar radiation was much larger in magnitude than the whole China [6].

On the other hand, further examination of the surface water vapors changes reveals that the surface solar radiation negatively correlates with the near surface water vapors, particularly in dry and high regions [3]. The authors from the same reference deduced that due to the absorption of solar radiation by the atmospheric water vapor, increases in water vapor cause decreases in surface solar radiation.

Although the variation of solar radiation could be attributed to various impacting factors, the relationship between surface solar radiation changes and aerosol or water vapor changes are still under much debate[3]. Decreased in solar radiation still cannot be fully explained neither by the increase of aerosol loading nor decrease in water vapor. Thus, to provide a complete explanation on changes of solar radiation, more observational data is required from time to time.

Long term variation of solar insolation had been routinely investigated and widely studied in the literatures. However, parallel observations in short time scale variation were not frequently reported. This lacking could be associated with the limitation in the measurement technique. Therefore, a method for monitoring and analysis of short time scale variation ought to be developed. This information could be used in various fields including for weather prediction, real-time monitoring of surface vegetation, evapotranspiration studies and others[2]. This paper is aiming at filling this gap for frequent insolation prediction, and also for the investigation of short time scale changes of solar radiation due to aerosol loading and water vapor content. Also in this paper, the ground-based measurement technique using spectrometer is used. This is

because the method has higher accuracy, cost-effective in financial wise as well as high temporal resolution [7].

This paper is arranged in five sections. After this introduction, the theoretical background of this work is outlined in Section II. It is then followed by description of research methodology in Section III. Results and discussion are presented in Section IV and the paper is concluded in Section V.

II. THEORETICAL BACKGROUND

Measurements of atmospheric aerosols and water vapor in short time scale is implausible due to lack of frequent observation neither by satellite nor ground base stations. Therefore, collected solar spectrum is separated into three segments (UV, PAR, and NIR) and the corresponding temporal changes of their fraction to global is used to exemplify the variations of aerosols and water vapor in short time scale.

Evolution of UV, PAR, and NIR components of the solar spectrum is obtained by computing the fraction of each component to global solar radiation. It is determined by integrating the corresponding spectral segment in regards to the total measured:

$$F_n = \frac{\int_{\lambda_{n,1}}^{\lambda_{n,2}} I(\lambda)d\lambda}{\int_{\lambda_1}^{\lambda_2} I(\lambda)d\lambda}, \quad (1)$$

where I and λ are the measured intensity and wavelength, respectively. Subscript n denotes the corresponding spectral component. In our division, fraction of UV, PAR, and NIR are estimated in the range of 289.71 to 400nm, 400 to 700nm, and 700-995.26nm, respectively. The small spectral resolution (<0.1nm) allows accurate determination of definite integral using trapezoid rule of integration:

$$\int_{\lambda_1}^{\lambda_2} I(\lambda)d\lambda = \frac{1}{2}[I(\lambda_1) + I(\lambda_2)][\lambda_2 - \lambda_1] \quad (2)$$

To avoid cloudy points from the entire data set, only spectrums with Du Mortier's nebulosity index (NI) and Perez's clearness index (ε) greater than 0.92 and 1.55, respectively are selected for further analysis. Both threshold values are pre-determined by Langley-plot analysis where corresponding indexes that give the highest correlation represent the most likely clear and stable atmosphere. The respective algorithms for NI computation are shown as follows [8]:

$$NI = \frac{1 - I_d/I_g}{1 - CR}. \quad (3)$$

The cloud ratio, CR is given as:

$$CR = \frac{I_{d,cl}}{[I_{d,cl} - \exp(-4mAr)\sin\alpha]}, \quad (4)$$

here $I_{d,cl}$ represents the clear sky illuminance given by:

$$I_{d,cl} = 0.0065 + (0.255 - 0.138\sin\alpha)\sin\alpha, \quad (5)$$

$$Ar = \left\{5.4729 + m\left[3.0312 + m\left\{-0.6329 + m(0.091 - 0.00521m)\right\}\right]\right\}^{-1}, \quad (6)$$

where Ar is the Rayleigh scattering coefficient, m is the optical air mass and α is the solar altitude. The Perez's model of clearness index, ε is calculated by [9]:

$$\varepsilon = \left(\frac{(I_{ed} + I_{dir})/I_{ed} + 1.041\Phi_H}{1 + 1.041\Phi_H}\right) \quad (7)$$

where I_{dir} is the direct irradiance and Φ_H is the solar zenith angle in radian.

III. SITE AND MEASUREMENT

The solar spectrums were collected at an urban area of Kota Kinabalu, Tun Mustapha Tower (116°E, 6°N, 7.844m above sea level) from 1st April to 31st May 2012. This site was selected because it has a clear view of sunrise to ensure that the solar pathway is not blocked by irrelevant objects or artificial buildings. The global solar radiation, I_G was measured by LR-1 spectrometer (ASEQ, Canada). Table I presents the range of detectable wavelength and other important specifications of the unit.

TABLE I
SPECIFICATIONS OF ASEQ LR-1 SPECTROMETER

Specifications	ASEQ LR-1 Spectrometer
Detector range	300 – 1100 nm
Resolution	< 3 nm (with 200 um fiber)
Pixels	3648
Pixel size	8 um x 200 um
Pixel well depth	100,000 electrons
Signal-to-noise ratio	300:1
A/D resolution	14 bit
Fiber optic connector	SMA 905 to 0.22 numerical aperture single strand
Exposure time	2.5 ms – 10 s
CCD reading time	14 ms

Measurements were taken for every 3 minutes average. The analysis interval for each day was selected by the air mass range from 2 to 6. This range of air mass was typically associated to the hours just after sunrise from 0640 to 0815 hours. For lower air masses, they are not used because the rate-of-change of air mass and solar irradiance is small, failed to exemplify the variation of solar irradiance in long defined

range. Besides that, only morning values are used because the afternoon hours are often cloudy and overcast. On the other hand, higher air masses are avoided due to greater uncertainty in air mass caused by refraction corrections that are increasingly sensitive to atmospheric temperature profiles [10].

In our processing, air mass, *m* is calculated based on geometrical solar zenith angle, which is calculated based on Solar Position Calculator, provided by Institute of Applied Physics of the Academy of Science of Moldova.

The temporal evolution of the respective fractions to global was obtained directly using the measured spectrum in pixels. Each pixel measured by the unit in a given wavelength has an intensity value represented by a digital number. Though it is not radiometrically calibrated, rationing both spectral segments yields a unitless parameter. Therefore, analysis of fraction of UV, PAR, and NIR to global radiation can utilize the raw data in pixels. However, in comparisons between the predicted and reference value of irradiance obtained from radiative transfer code, Langley calibrated value was used. Details of the Langley calibration procedure are discussed elsewhere in [10, 11]. The implications of the corresponding temporal changes of the respective fractions to global radiation on Langley-plot analysis will be discussed in Section IV Part C.

IV. RESULTS AND DISCUSSION

A. Analysis of Fraction of UV, PAR, and NIR to Global

Prior to the data analysis, the collected solar spectrums were fed to an objective algorithm to select data points from a continuous time series that exhibit only clear sky condition. This algorithm uses the Perez-Du Mortier sky classification model to filter out cloudy and overcast data points (refer Section II). The purpose to perform this filtration is to eliminate and reduce the effects of cloud cover or transits on attenuation of solar radiation measured at ground surface.

Fig. 1 shows the frequency distribution of UV, PAR, and NIR fractions of G measured from air mass 2 to 6 over the study area after the filtration procedure. The fractions varied from 3.3 to 4.8% for UV/G, 72.1 to 81.2% for PAR/G, and 14.4 to 22.8% for NIR/G. The frequency distribution follows a Gaussian distribution and the fraction corresponding to the maximum frequencies (3.6-3.9% for UV/G, 77.3-78.6% for PAR/G, and 17.2-18.6% for NIR/G) matches the mean fraction indicated in Table II.
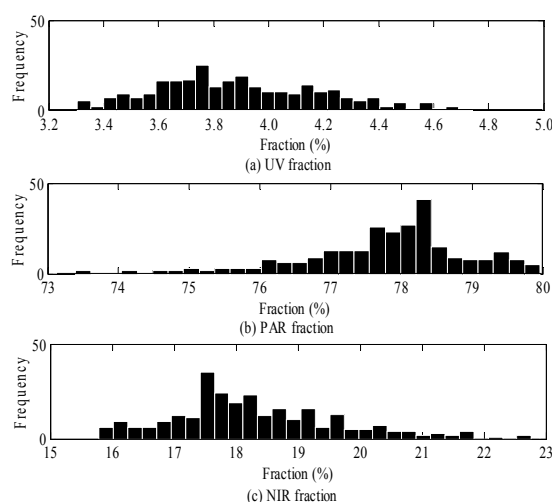

Fig. 1 Frequency distribution of (a) UV, (b) PAR, and (c) NIR fraction to Global

Broader amplitude of fraction occurs in PAR and NIR because they incorporate short time scale variation of aerosol and water vapor. Low variance in UV fraction is expected because daily averaged ozone concentration deviates only by very small amount, smaller deviation should be expected in diurnal evolution. Higher variance in NIR is associated to the possible change of relative humidity and temperature for decreasing air mass from 2 to 6; causing the concentration of water vapor changes notably. Aerosol mass loading is the dominant factor responsible for attenuation of solar radiation in PAR region. This indicates that variation of aerosol loading has considerable effects on solar radiation but its effects are relatively less momentous compared to total atmospheric water vapor columnar.

TABLE II
STATISTICAL PROPERTIES OF G,UV, PAR, AND NIR OBSERVED BETWEEN
1ST APRIL TO 31ST MAY 2011 OVER THE STUDY AREA

Radiation component	Fraction to global (%)	Standard deviation	Mean (pixels)	Maximum (pixels)
UV	3.90E+00	3.01E-01	3.54E+04	2.45E+05
PAR	7.78E+01	1.20E+00	5.62E+05	4.02E+06
NIR	1.83E+01	1.37E+00	9.74E+04	9.16E+05
Global	-	-	3.79E+06	5.18E+06

B. Evolution of UV, PAR, and NIR fraction to Global

Fig. 2 presents the diurnal evolution of each segment to global radiation ranges from air mass 2 to 6. Evolution pattern over time for UV and PAR shared a similar pattern such that it increases with decreasing air mass. This is expected because the solar optical path length reduces for decreasing air mass, which in turn causes less attenuation of solar radiation either by absorption or scattering due to gaseous particles or air molecules.
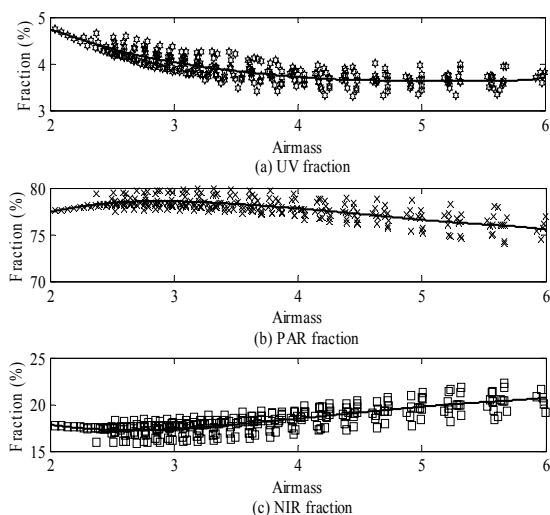
Fig. 2 Evolution of (a) UV, (b) PAR, and (c) NIR fraction for air mass ranges from 2 to 6

However, a different pattern is observed in NIR fraction; it decreases when air mass reduces. One possible explanation for this pattern is likely corresponding to increase of atmospheric water vapor presented in air. NIR wavelengths are highly absorptive by water vapor and thus presence of great amount of which subsequently causes reduction of NIR in solar spectrum [12]. Similar results were also reported by [3] that due to the absorption of solar radiation by the atmospheric water vapor, increases in water vapor will cause decrease in surface solar radiation.

Given that water vapor absorbs more G than UV therefore higher UV fraction could be associated to the presence of higher atmospheric water vapor content [1]. Similar deduction could be applied on PAR and NIR fraction where water vapor absorbs more NIR than PAR hence simultaneous higher PAR and lower NIR fraction could be related to the presence of higher water vapor concentration. The statistical investigations of the present data support this premise that increasing trend of PAR fraction matches the decreasing trend of NIR fraction (Fig. 2). The decreasing trend in NIR fraction implies that as air mass decreases in time evolution, rate of extinction in NIR wavelengths increases in proportion due to increasing amount of water vapor.
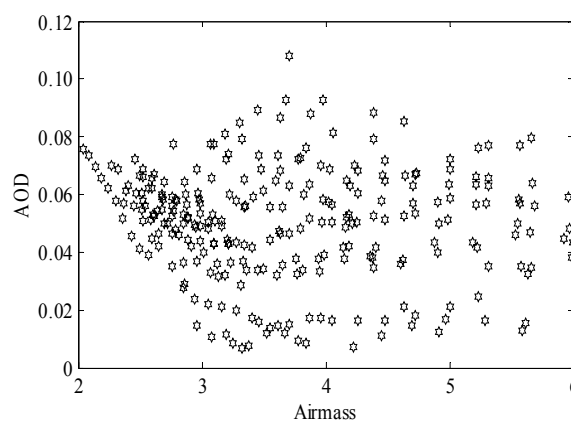

Fig. 3 Variation of AOD at wavelength 550nm for changing air mass during the measurement period

Another interesting trend is observed that the negative slope in PAR fraction at air mass 3 (Fig. 2) does not correspond to steeper increase in NIR. Instead it is associated to the increase of aerosol loading. The increasing trend of aerosol optical depth after air mass 3 matches the decreasing trend in PAR fraction (Fig. 3). Noted that the direct solar beam is also strongly affected by aerosol amount, presence of which in great amount significantly attenuates solar radiation either by absorption or scattering. Therefore, the steeper slope of decrease in PAR fraction at air mass 3 should be regarded of increasing amount of aerosols but not from the effects of water vapor.

Till this end, the prevailing justifications suggested that the variation of atmospheric water vapor in small scale time evolution is most significant in air mass ranges from 3 to 6, which is corresponding to times just after sunrise. This is within the expectation because sun rise heats up the atmosphere, causing rate of evaporation increases accordingly and leading to higher amount of water content. Also deducible in the variation of this parameter affects most in NIR wavelengths (16.48-20.69%), relatively lower in PAR (83.69-86.50%), and the least in UV (3.47-4.06%). This finding is also in good agreement with [13] that in more humid conditions, absorption of solar radiation in the NIR region of the solar spectrum is enhanced, whereas absorption in the UV region does not vary significantly.

C. Implications of Evolution of UV, PAR, and NIR fraction to Global on Langley-Plot Analysis

Langley-plot analysis is a method to measure the sun's irradiances with ground-based instruments that based on repeated measurements operated at a given location for a cloudless situation. A successful Langley plot is imperative to permit extrapolation of the regression line to zero air mass that further allows the determination of the instrument output at top of atmosphere. This value when divided by extraterrestrial constant at given wavelength yields the radiometric calibration factor. The accuracy of this factor strongly depends on a cloudless and stable atmosphere with less variation in aerosol loading and water vapors content.

In our parallel work, we found that the mean bias difference (MBD) of the Langley calibration factor is inconsistent under different atmospheric condition. Fig. 4 shows that on high turbidity day(Fig. 4(a)),all wavelengths exhibit consistent pattern that the bias reduces for decreasing air mass except for 865nm where its bias is over 30% regardless of air mass. As for low turbidity day, the pattern is inconsistent that the bias reduces for decreasing air mass from 6 to 3 and begins to deviate beyond air mass 3 (Fig. 4(b)).
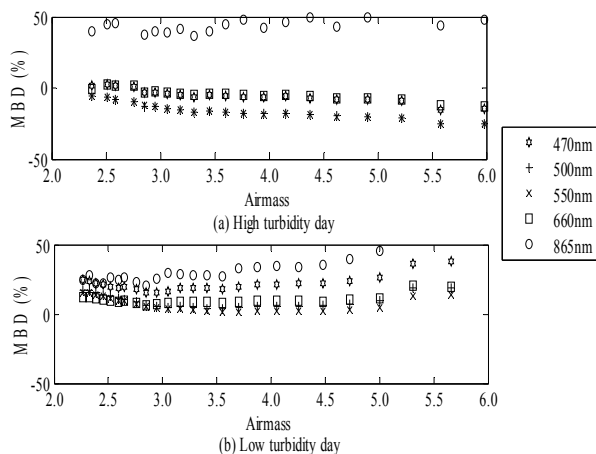

Fig. 4 Performance of Langley calibrated results for (a) high turbidity day (b) low turbidity day

Detailed inspection of the corresponding daily evolution of UV, PAR, and NIR fractions to global radiation suggests that variation of aerosol and water vapors content could be responsible for inaccurate Langley calibration factor obtained in the parallel work. Fig. 5 presents the evolution of each segment for the two different turbidity days. It is observed that the high turbidity day with unusual high MBD at 865nm (NIR) remarked the higher UV and PAR fraction but lower in NIR. Given that attenuations of solar radiation by water vapor is most significant in NIR and relatively lesser in PAR and UV fraction [1]. Therefore, simultaneous higher fraction in UV/PAR and lower fraction in NIR is likely associated to increase of water vapor that strongly attenuates the solar radiation in NIR wavelengths; resulting an unusual high MBD at 865nm for the day.
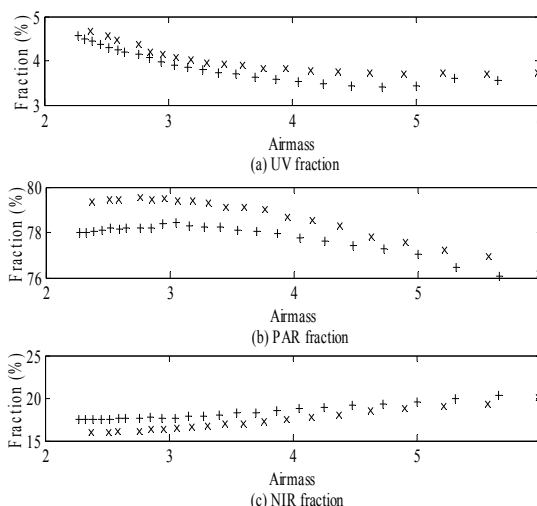

Fig. 5 Diurnal evolution of (a) UV, (b) PAR, and (c) NIR fraction for the two different turbidity days. Symbol + and x represents low and high turbidity day, respectively

Although the contribution of water vapor were taken into account when simulating the reference value from the radiative transfer code, their distinct variation in short time scale is however neglected as there is no available data for hourly or shorter time range inspection.

Deviation of MBD pattern for all wavelengths on low turbidity day is likely related to effects from variation of aerosol loading. Fig. 6 shows that comparatively AOD varies more significantly on low turbidity day, from 0.01 to 007 when compared with high turbidity day, especially after air mass 3. Even short time scale aerosol variation could have large enough effects to attenuate the solar radiation. This variation however does not take into account when simulating the reference value because daily average turbidity coefficient was used due to lack of complementary meteorological measurement.
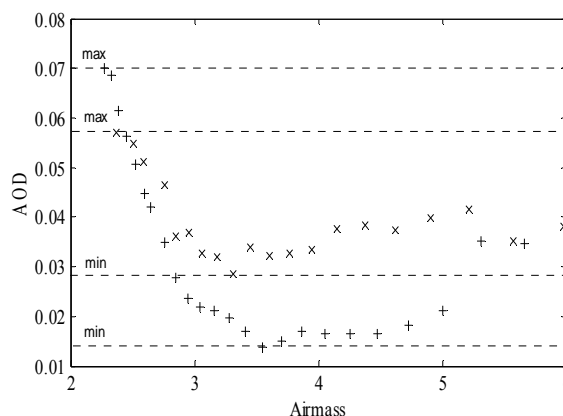

Fig. 6 Diurnal variation of AOD at wavelength 550nm for the two different turbidity days. Symbol + and x represents low and high turbidity day, respectively

V. CONCLUSION

In this study, short time scale changes of solar radiation in ultra violet (UV), photosynthetic active radiation (PAR), and near infrared (NIR) wavelengths,for air mass ranges from 2 to 6were investigated. Ground-based method using spectrometer was used for data collection. In general, it was found that UV fraction to global irradiance varies the least, followed by PAR and NIR in this short time scale analysis. Detail inspection shows that UV and PAR fraction increases for decreasing air mass from 6 to 3 whereas NIR decreases for the same air mass evolution which is believed to be due to increasing in water vapors content (water vapors content increased as air mass reduced from 6 to 3). This observation is consistence with the mean bias difference (MBD) value in the Langley plot analysis where MBD value for NIR (865nm) on high turbidity day (which is corresponding to high water vapors content) is higher compared to on the low turbidity (corresponding to lower water vapors content) day. Beyond air mass 3 (between 3 to 2), PAR (550nm) was reducing (as the aerosol loading increases) and NIR was almost constant (as the water vapors content insignificantly varies) whereas UV was found to further increased (less affected by aerosol loading and water vapors content). Deviation ofMBDpattern in the Langley-plot analysis for almost all wavelengths for low turbidity day shows the dominant effects of the aerosol loading (aerosol effects).

REFERENCES

[1] J. F. Escobedo, E. N. Gomes, A. P. Oliveira, and J. Soares, "Ratios of UV, PAR and NIR components to global solar radiation measured at Botucatu site in Brazil," Renewable Energy, vol. 36, no. 1, pp. 169–178, Jan. 2011.

[2] J.-M. Yeom, K.-S. Han, and J.-J. Kim, "Evaluation on penetration rate of cloud for incoming solar radiation using geostationary satellite data," J. Atmos. Sci., vol. 48, no. 2, pp. 115–123, May 2012.

[3] C. Wang, Z. Zhang, and W. Tian, "Factors affecting the surface radiation trends over China between 1960 and 2000," Atmos. Environ., vol. 45, no. 14, pp. 2379–2385, 2011.

[4] R. T. Pinker, B. Zhang, and E. G. Dutton, "Do satellites detect trends in surface solar radiation?," Science, vol. 308, pp. 850–854, May 2005.

[5] Y. Qian, D. P. Kaiser, L. R. Leung, and M. Xu, "More frequent cloud-free sky and less surface solar radiation in China from 1955 to 2000," Geophys. Res. Lett., vol. 33, L01812, pp. 1–4, 2006..

[6] W.-J. Tang, K. Yang, J. Qin, C. C. K. Cheng, and J. He, "Solar radiation trend across China in recent decades: a revisit with quality-controlled data," Atmos. Chem. Phys. Discuss. vol. 10, pp. 18389–18418, Aug. 2010.

[7] J. H. W. Chang, J. Dayou, and J. Sentian, "Diurnal evolution of solar radiation in UV, PAR and NIR bands in high air masses (Accepted for publication)," Nat. Env. Poll. Tech., to be published.

[8] A. Zain-Ahmed, K. Sopian, Z. Z. Abidin, and M. Y. H. Othman, "The availability of daylight from tropical skies — a case study of Malaysia," Renewable Energy, vol. 25, pp. 21–30, 2002.

[9] H. Djamila, C. C. Ming, and S. Kumaresan, "Estimation of exterior vertical daylight for the humid tropic of Kota Kinabalu city in East Malaysia," Renewable Energy, vol. 36, no. 1, pp. 9–15, Jan. 2011.

[10] L. Harrison and J. Michalsky, "Objective algorithms for the retrieval of optical depths from ground-based measurements," Appl. Opt., vol. 33, no. 22, pp. 5126–32, Aug. 1994.

[11] J. Slusser, J. Gibson, B. David, D. Kolinski, P. Disterhoft, K. Lantz, and A. Beaubien, "Langley method for calibrating UV filter radiometer," J. Geophys. Res., vol. 105, no. D4, pp. 4841–49, 2000.

[12] G. Lombardi, E. Mason, C. Lidman, A. O. Jaunsen, and A. Smette, "A study of NIR atmospheric properties at Paranal Observatory," Astron. Astrophys., vol. 43, pp. 1–7, 2011.

[13] X. Xia, Z. Li, P. Wang, M. Cribb, H. Chen, and Y. Zhao, "Analysis of relationships between ultraviolet radiation (295 – 385 nm) and aerosols as well as shortwave radiation in North China Plain," Ann. Geophys., vol. 26, pp. 2043–2052, 2008.